MIT Libraries | DSpace@MIT

MIT Open Access Articles

Nonlocal Detection of Out-of-Plane Magnetization in a Magnetic Insulator by Thermal Spin Drag

The MIT Faculty has made this article openly available. ***Please share*** how this access benefits you. Your story matters.

Citation: Avc, Can Onur et al. "Nonlocal Detection of Out-of-Plane Magnetization in a Magnetic Insulator by Thermal Spin Drag." Physical review letters 124 (2020): 027701 © 2020 The Author(s)

As Published: http://dx.doi.org/10.1103/PhysRevLett.124.027701

Publisher: American Physical Society

Persistent URL: https://hdl.handle.net/1721.1/125371

Version: Final published version: final published article, as it appeared in a journal, conference proceedings, or other formally published context

Terms of Use: Article is made available in accordance with the publisher's policy and may be subject to US copyright law. Please refer to the publisher's site for terms of use.

Massachusetts Institute of Technology

Editors' Suggestion

Nonlocal Detection of Out-of-Plane Magnetization in a Magnetic Insulator by Thermal Spin Drag

Can Onur Avci,[1,2,*] Ethan Rosenberg,[1] Mantao Huang,[1] Jackson Bauer,[1] Caroline A. Ross,[1] and Geoffrey S. D. Beach[1]

[1]Department of Materials Science and Engineering, Massachusetts Institute of Technology, Cambridge, Massachusetts 02139, USA

[2]Department of Materials, ETH Zürich, CH-8093 Zürich, Switzerland

(Received 5 July 2019; revised manuscript received 24 October 2019; published 17 January 2020)

We demonstrate a conceptually new mechanism to generate an in-plane spin current with out-of-plane polarization in a nonmagnetic metal, detected by nonlocal thermoelectric voltage measurement. We generate out-of-plane (∇T_{OP}) and in-plane (∇T_{IP}) temperature gradients, simultaneously, acting on a magnetic insulator-Pt bilayer. When the magnetization has a component oriented perpendicular to the plane, ∇T_{OP} drives a spin current into Pt with out-of-plane polarization due to the spin Seebeck effect. ∇T_{IP} then drags the resulting spin-polarized electrons in Pt parallel to the plane against the gradient direction. This finally produces an inverse spin Hall effect voltage in Pt, transverse to ∇T_{IP} and proportional to the out-of-plane component of the magnetization. This simple method enables the detection of the perpendicular magnetization component in a magnetic insulator in a nonlocal geometry.

DOI: 10.1103/PhysRevLett.124.027701

In a magnetic insulator (MI), a temperature gradient (∇T) can generate a spin Seebeck effect (SSE), i.e., a pure spin current flow along the gradient direction with spin polarization ($\boldsymbol{\sigma}$) parallel to the magnetization unit vector $\mathbf{m}$ [1–8]. The SSE can be detected electrically if the spin current is injected into an adjacent conducting layer that hosts a spin-to-charge conversion mechanism, such as the inverse spin Hall effect (ISHE) in a heavy metal [9]. In this case, the ISHE leads to a voltage V_{ISHE} that can be exploited for, e.g., spin Seebeck power generation [10,11] and detection of the magnetic state in insulators for potential spin-caloritronics memory and logic devices [12]. However, since $V_{\mathrm{ISHE}} \propto |\nabla T \times \mathbf{m}|$ [4,5,13], a voltage is only generated when the spin current direction and spin polarization are noncollinear, limiting the measurement geometry and the detectable magnetization components in devices. Most research has focused on MI-heavy metal bilayers with in-plane magnetization and out-of-plane temperature gradient, which gives rise to a lateral voltage across the heavy metal layer sensitive to the rotation of $\mathbf{m}$ about ∇T [14,15]. This allows for a simple local geometry, but precludes detection of out-of-plane magnetization. In similar devices, the magnetization vector can also be probed electrically via spin Hall magnetoresistance (SMR), which allows detection of both in-plane and out-of-plane magnetization components by Hall voltage measurements [16–19]. However, so far, no means for nonlocal thermally driven spin signal detection of the out-of-plane magnetization component has been proposed or realized experimentally.

Here we demonstrate that by using an engineered local temperature gradient one can detect the out-of-plane magnetization of a MI by simply measuring the transverse voltage drop across the Pt strip placed on top. A local heat source near the strip generates out-of-plane (∇T_{OP}) and in-plane (∇T_{IP}) temperature gradients, resulting in pure spin currents that produce a superposition of several $\mathbf{m}$-dependent voltages along the Pt detector channel. By rotating $\mathbf{m}$ in plane we reveal that ∇T_{OP} gives rise to ISHE voltage due to the SSE, and ∇T_{IP} generates a spin Nernst magnetoresistance (SNMR) [20], similar to the SMR but the charge current is driven by a temperature gradient rather than an applied voltage and the spin current generation relies on the spin Nernst effect [21–23] rather than the spin Hall effect. Surprisingly, we also measure a large signal proportional to the perpendicular component of $\mathbf{m}$, too large to be accounted for by the anomalous Hall effect (AHE) component of the SNMR. We explain the phenomenon by the combined action of ∇T_{OP} and ∇T_{IP}, where ∇T_{OP} generates a magnonic spin current injection from MI into Pt with out-of-plane polarization and ∇T_{IP} drags the spin-polarized current in plane, against the gradient direction. Ultimately, this generates a voltage orthogonal to both ∇T_{IP} and ∇T_{OP} due to the ISHE of the spin-polarized current drag. Recently, perpendicularly magnetized MIs have come into focus since they are advantageous for devices based on spin-orbit torque switching and domain wall motion [24–28]. By enabling quantification of SSE, SNMR, and the out-of-plane component of magnetization, these findings mark a significant step toward efficient generation,

 © 2020 American Physical Society

manipulation, and nonlocal detection of magnonic spin currents in MIs.

We grew two TmIG thin films of 6.1 and 8.5 nm thicknesses by pulsed laser deposition on a 0.5-mm-thick (111) GGG ($Gd_3Ga_5O_{12}$) substrate [29] with saturation magnetization of 110 kA/m. Epitaxial growth of the TmIG films was confirmed via a high-resolution x-ray diffraction 2θ-ω scan of the (444) reflection, and the film thicknesses were measured using x-ray reflectivity. The first as-grown film had perpendicular magnetic anisotropy of magnetoelastic origin [29,30], but after lithographic processing to form Au and Pt strips, the easy axis reoriented in plane, attributed to strain relaxation. The second film retained perpendicular anisotropy after lithography. The easy-plane anisotropy of the first sample was convenient for the present experiments as it facilitated the measurement of mostly in-plane magnetization-related thermoelectric signals such as SSE and SNMR. The second perpendicularly magnetized sample served as a confirmation of the out-of-plane-related signal as described later. On top of the TmIG, we defined a 3-μm-wide and 200-μm-long Au(66 nm)/Ta(3 nm)/TaO_x(~10 nm) "heater" channel and a Pt (4 nm) "detector" channel separated by a distance (d) using electron beam lithography and magnetron sputtering, followed by lift-off [see Fig. 1(a)]. Both channels were terminated by large (120×80 μm^2) contact pads on both sides, allowing electrical connection by wire bonding. The sample is glued on a sample holder made of large gold pads serving as heat sink. We injected an ac current (I_{ac}) with frequency $\omega/2\pi = 10$ Hz and variable amplitude through the heater, and detected the harmonic voltage across the Pt channel during either a magnetic field sweep or angular rotation of the sample in a constant magnetic field. Definition of the coordinate system and in-plane angle can be found in Fig. 1(b). All measurements were performed in ambient conditions.

A high amplitude current injection through the heater channel increases the temperature locally due to Joule heating. Since the substrate is a much better thermal conductor than the surrounding air, the heat dissipation occurs predominantly through the substrate, giving rise to both out-of-plane (∇T_{OP}) and in-plane (∇T_{IP}) temperature gradients, as depicted in Fig. 1(b), lower panel. The 10-nm-thick TaO_x between the Au/Ta and the MI ensures that no spin current is injected into the MI by the spin Hall effect of Au/Ta (see Supplemental Material, Section SM.1 [31]); therefore, spin Hall originated magnon generation and its long-range transport cannot occur, in contrast to the cases of Refs. [32–34]. We, therefore, expect thermoelectric voltages driven predominantly by the local temperature gradients within the Pt stripes and the TmIG underneath.

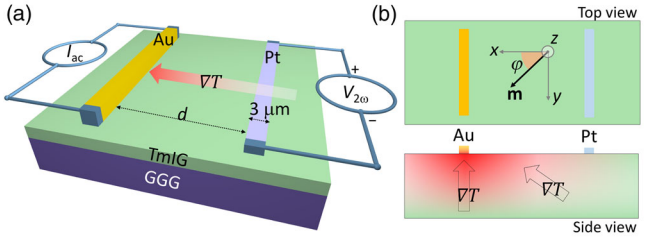

FIG. 1. (a) Device schematics and electrical connections (not to scale). (b) Top and side view of a representative device and coordinate system. Shaded red color in the lower panel of (b) indicates the presumed heat distribution upon current injection through the Au heater layer.

We first focus on the voltages that arise from the in-plane component of $\mathbf{m}$, and show that the data exhibit the conventionally expected behaviors. In Fig. 2(a) we show the second harmonic voltage ($V_{2\omega}$) measured by rotating the sample in plane in an external field of $\mu_0 H = 500$ mT. We note that the Joule heating, and hence the temperature gradient, scales with I^2. Therefore, the thermoelectric voltages due to ∇T are expected to appear in the second harmonic voltage $V_{2\omega}$ [15,32,35]. The different signals (manually offset for clarity) correspond to different heater-detector pairs with d varying between 20 and 80 μm, measured by applying an ac current $I = 50$ mA, corresponding to $j = 1.7 \times 10^{11}$ A/m^2 (rms). We observe an angular-dependent signal that decays with increasing d, which is expected to be composed of two sources of thermoelectric voltage: the ISHE voltage due to the SSE (V_{SSE}) driven by ∇T_{OP} and the SNMR voltage (V_{SNMR}) due to ∇T_{IP}. The angular dependence of $V_{2\omega}$ due to these two components follows $V_{2\omega} = V_{SSE}\nabla T_{OP}\cos\varphi\sin^2\theta + V_{SNMR}\nabla T_{IP}\sin 2\varphi\sin^2\theta$, where θ is the magnetization angle with respect the z axis. The experimental data are well fitted by this expression [Fig. 2(a)] and setting $\sin^2\theta = 1$ (as $\mathbf{m}$ is constrained to the xy plane), allowing us to quantify V_{SSE} and V_{SNMR}. As a cross-check, we measure the SSE contribution with a field sweep, since V_{SSE} is odd under 180° magnetization reversal, which should result in a signal jump upon field reversal. Figure 2(b) shows such measurements for $d = 30$ μm. We see clear steps reflecting magnetization reversal whose amplitude depends on the applied field angle. We plot the amplitude of steps (divided by 2) in these and other measurements (not shown) in Fig. 2(c). We see that the signal is proportional to $\cos\varphi$, which clearly reflects the SSE origin. Moreover, the amplitude of the SSE signal inferred from Fig. 2(b) is in excellent agreement with that obtained from fitting in Fig. 2(a). This finally allows us to conclude that the data in Fig. 2(a) predominantly arise from the SNMR and the SSE.

These findings demonstrate the coexistence of substantial ∇T_{OP} and ∇T_{IP} acting on the detector channel, which will be important for the interpretation of the experimental results discussed later. For a cross-check, we have additionally performed measurements on devices with two heater layers placed on both sides of the detector channel. The results shown in the Supplemental Material (Section SM.2) [31] further confirm the proposed temperature gradient

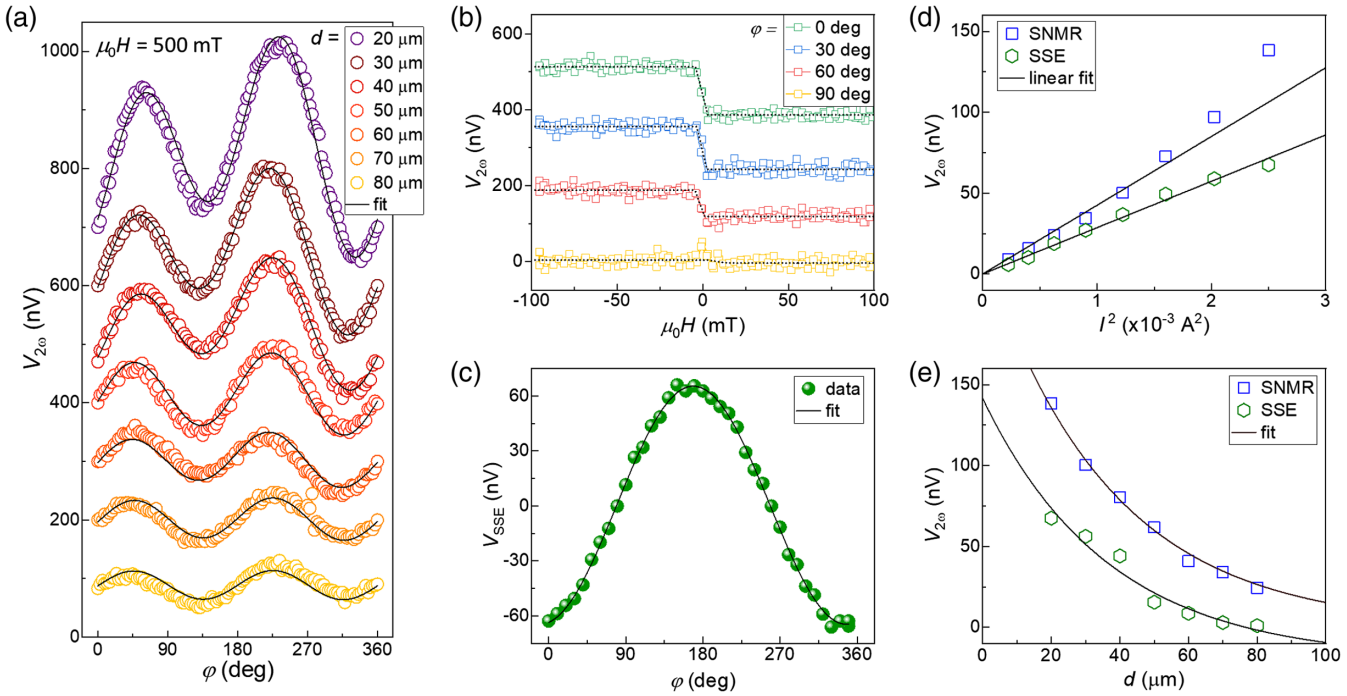

FIG. 2. (a) Second harmonic voltages recorded with a heater current of $I_{ac} = 50$ mA during a φ rotation in a constant external field $\mu_0 H = 500$ mT of devices with different heater-detector separation d. (b) In-plane field sweep measurements for different angles φ, where the signal jumps are associated with the SSE. (c) Angular dependence of the SSE signal and the fit following the expected $\cos\varphi$ function. Current (d) and heater-detector distance (e) dependence of the SNMR and the SSE signals and associated fits. Signals in (a) and (b) are manually offset for clarity.

scenarios and the SSE and SNMR signals associated with them. Furthermore, we have performed temperature-dependent resistivity measurements to quantify the amplitude of the in-plane temperature gradients and have found that ∇T_{IP} decays exponentially as a function of d and reaches up to 1 K/μm for the device with the closest heater-detector distance (see Supplemental Material, Section SM.3 [31]). We note that due to the width of the detection channel (3 μm), variations of ∇T_{IP} within the channel itself can be safely neglected and an average value can be used for further analysis.

Next, we analyze the I and d dependence of the SNMR and SSE signals. In Fig. 2(d) we plot the signals as a function of I^2 since ∇T and consequently the thermoelectric signals are expected to scale with I^2, as mentioned earlier. We observe that both the SNMR and the SSE signals scale linearly with I^2 up to moderate current densities, but the SNMR signals show a slight deviation from the linear trend at higher currents due presumably to the temperature dependence of this effect and strong Joule heating of the device at these current densities. Nevertheless, we find reasonable agreement between the measurement and the expected trends. In Fig. 2(e) we plot both signals as a function of d for a constant current. Both signals decay nearly exponentially with d (as estimated in the Supplemental Material, Section SM.3 [31]), confirming their thermal origin.

We now turn to contributions to the measured voltage related to the out-of-plane component of $\mathbf{m}$ (m_z), which include a component that is unique to the present nonlocal experimental geometry. By symmetry, neither SSE nor the SNMR is sensitive to a reversal of the magnetization vector from $\theta = 0°$ to $\theta = 180°$, or vice versa, since $\sin^2\theta = 0$ in both cases. Figures 3(a) and 3(b) show $V_{2\omega}$ measured while sweeping an out-of-plane field H_z. For the in-plane sample, due to the shape anisotropy of the TmIG ($M_s = 110$ kA/m), the field to saturate the magnetization out of plane is ~140 mT, above which $\mathbf{m}$ is expected to align with $\mu_0 H_z$, while in the perpendicularly magnetized sample we expect sharp reversal of the signal around $\mu_0 H_z = 0$. In both cases, we observe a clear signal that changes as a function of heater current amplitude. In these data, we identify two effects. The first one is a linear, field-induced signal due to the ordinary Nernst-Ettinghausen effect of Pt driven by ∇T_{IP}. The second one is the difference between the negative and positive high field voltage, which follows m_z. Analysis of this $\mathbf{m}$-dependent signal as a function of I [Fig. 3(c)] shows that the signal scales approximately as I^2 as expected of a voltage of thermoelectric origin. Moreover, for the in-plane sample we plot $V_{2\omega}$ vs d, and similarly to SSE and SNMR signals, we find that this signal exponentially decays as a function of d [Fig. 3(c), inset]. These measurements unequivocally show the presence of a thermoelectric signal following m_z.

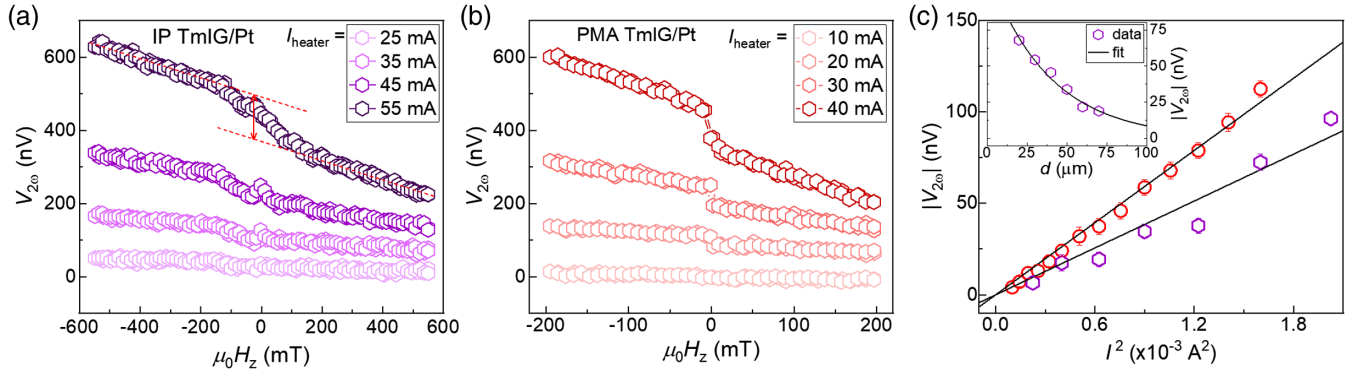

FIG. 3. (a) Second harmonic voltage in in-plane magnetized TmIG/Pt upon out-of-plane field sweep for different heater currents for $d = 30$ μm. A field-induced linear slope, which we associate with the ordinary Nernst effect of Pt, and a m_z-dependent signal (gap between the two saturated states shown by the red arrow) are observed. (b) The same measurement configuration reported in (a) performed on a separate perpendicularly magnetized TmIG/Pt sample with $d = 10$ μm. (c) The current dependence of the m_z-dependent signal and fit following $V_{2\omega} \propto I^2$ for both samples. Inset: Heater-detector distance dependence of the m_z-dependent signal for IP TmIG/Pt sample and exponential fit. Signals in (a) and (b) are manually offset for clarity.

An m_z-dependent signal due to the thermal counterpart to the anomalous Hall-like component of the SMR may be expected to give rise to the data reported in Fig. 3, but we demonstrate that this is not the case here and the signal has predominantly a different origin. We show this by comparing the thermoelectric data to electrical Hall effect measurements in a separate Hall cross device fabricated near the actual device on the same in-plane TmIG/GGG film. First, we show the φ-scan thermal [Fig. 4(a)] and electrical [Fig. 4(b)] signals driven by ∇T_{IP} and I, respectively (we subtract the SSE contribution related to ∇T_{OP} in the former case). We see that these two signals look identical except for the difference in their amplitudes. Now, we focus on the m_z-dependent signals after subtraction of the linear slope due to the ordinary Nernst-Ettinghausen (Hall) effect in the thermal (electrical) measurements [Figs. 4(c) and 4(d)]. We observe that there is a large difference in the amplitudes of the m_z-dependent signals relative to the respective SNMR and SMR signals. In the thermal case, for instance, the step height is 120 ± 10 nV, which is ~55% of the SNMR signal shown in Fig. 4(a). However, in the electrical case, the step height is 3 ± 2 μV, which is ~6% of the SMR signal shown in Fig. 4(b), similar to previously reported ratios for this system [19,24]. If the driving mechanisms were solely the SNMR and SMR in thermal and electrical measurements, respectively, then we would expect the ratio of AHE-like signals to the SNMR and SMR to be the same in both cases. We can also rule out the effect of a proximity-induced contribution to anomalous Hall and Nernst effects in Pt since it will show up in both measurements due to their common origin through the Mott relation [36]. Moreover, it is now established that insulating magnetic materials in contact with Pt produce a negligibly small proximity effect at room temperature and the corresponding magnetoelectric signals are negligible, if any [4,37–39]. Therefore, the tenfold difference in the ratios indicates that the thermally driven AHE component of the SNMR cannot explain the signal in Fig. 4(e) by itself, and other contributions should be considered as discussed below.

Previously, we have shown that in and underneath the Pt detector channel, ∇T_{OP} and ∇T_{IP} coexist and that ∇T_{OP}

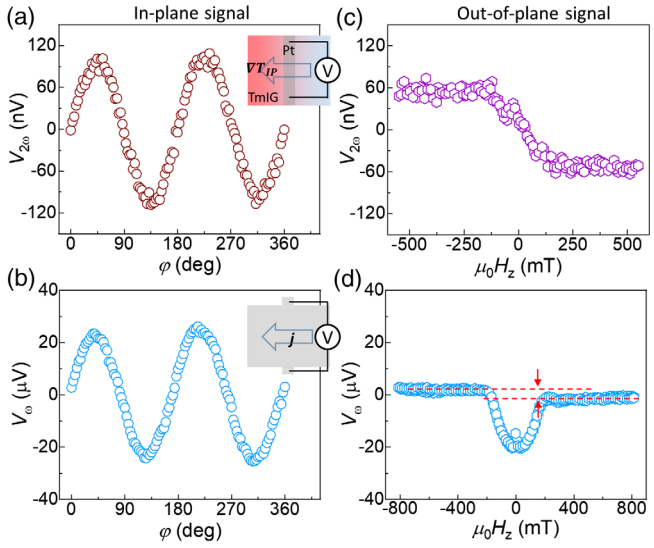

FIG. 4. Comparison of thermally driven (a),(c) and electrically driven (b),(d) voltage measurements. (a) The SNMR signal after subtraction of the SSE contribution due to ∇T_{OP}, centered on zero (measurement parameters $d = 30$ μm, $I_{ac} = 50$ mA). (b) The spin Hall magnetoresistance measured in identical condition on a nearby device by injection of $I_{ac} = 1.6$ mA. (c) The voltage recorded during an H_z sweep after subtraction of the linear field-induced slope [measurement parameters are the same as in (a)]. (d) The electrically driven Hall resistance signal with the H_z sweep after subtraction of linear slope due to ordinary Hall effect. In (d), at fields lower than the saturation field of **m** there is an additional signal due to the SMR becoming dominant as the **m** trajectory presumably leads to large SMR contribution in the electrical signal.

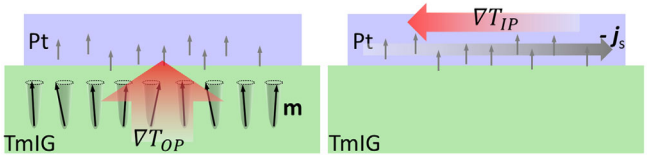

FIG. 5. Illustration of the thermal spin drag mechanism. ∇T_{OP} pumps thermally generated magnons into Pt (left), which creates an imbalance of spin population in favor of out-of-plane spins, and ∇T_{IP} acts as an electromotive force for the spin-polarized current and drags them toward the colder side (right). Finally, an ISHE voltage builds up orthogonal to both temperature gradients, which is the thermal spin drag voltage reported in Fig. 3.

can effectively pump thermally driven spin current into Pt. By the symmetry of the ISHE, the spin current pumped into Pt with out-of-plane polarization cannot produce an ISHE signal since the spin current direction and polarization are collinear. However, additionally, ∇T_{IP} may act as an electromotive force to drag the charge current against the gradient, as in the ordinary Seebeck effect. With the thermally driven spin pumping, the Pt is expected to be populated with more spins parallel to the magnetization of TmIG than antiparallel. Therefore, the in-plane current drag is predominantly spin polarized along **m**, which can generate an ISHE voltage orthogonal to both ∇T_{IP} and ∇T_{OP}. This ISHE signal is sensitive to m_z and can effectively contribute to the signal shown in Fig. 4(c). We illustrate this mechanism in Fig. 5 and identify this new effect as a "thermal spin drag," highlighting its origin. Assuming that the ratio between the AHE component of the SMR and the SMR itself remains the same for the thermoelectric counterpart, we conclude that the thermal spin drag is the dominant contribution to the m_z-dependent signal in nonlocal measurements and that its amplitude is comparable to that of ∇T_{OP}-driven SSE. For the data in Fig. 4(c) ($d = 30$ mm, $I = 50$ mA) and using characteristic transport parameters of Pt, we estimate that 0.12% of the free electrons are spin polarized due to the spin pumping from TmIG (see Supplemental Material, Section SM.3 [31]).

We should note that the sign and amplitude of the thermal spin drag signal will depend on several factors. First, if Pt were to be replaced by a material with an opposite sign of the spin Hall angle (such as W or Ta), the signal would reverse sign and its amplitude would scale with the spin Hall angle of the detector material. Also, the length of the Pt strip matters for the output voltage since the thermal spin drag effect generates an electric field, which is converted into a voltage linearly proportional to the channel length. Finally, we expect the thermal spin drag signal to strongly depend on the Pt thickness. Based on the description in Fig. 5, the laterally traveling spin current will be strongest near the interface and quickly decay away from it. If Pt is made thinner, the thermal spin drag signal should be enhanced due to much higher spin-polarized electron density per unit volume as the thickness approaches the spin diffusion length. However, for a full quantitative description of the thermal spin drag effect in ultrathin detector layers, surface and interface transport effects should be considered.

In conclusion, we studied thermoelectric voltages in a magnetic insulator TmIG/Pt bilayer driven by a nonlocal heat source and consequent temperature gradients. We identify three contributions to the second harmonic voltages related to **m** and driven by out-of-plane and in-plane temperature gradients: (i) the spin Seebeck effect (and consequently the ISHE) driven by ∇T_{OP}, (ii) the spin Nernst magnetoresistance and possibly its anomalous Hall counterpart driven by ∇T_{IP}, and, finally, (iii) the thermal spin drag followed by the ISHE driven by collective action of ∇T_{OP} and ∇T_{IP}. The dependence of these signals on heater current and distance shows very good agreement with their expected origins. The thermal spin drag effect, which we demonstrate here for the first time, reveals the complex interplay between heat, charge, and spin currents in devices that could generate useful signals to detect, e.g., the out-of-plane magnetization component in magnetic insulators. We note that due to the damping parameter α dependence of the SSE-driven spin pumping, we expect this signal to be further enhanced in MIs with lower α. Our study opens up new routes toward engineering temperature gradients to generate and manipulate thermal magnons and pure spin currents and detect magnetic states in MI-based spintronic devices.

This work was supported in part by SMART, one of seven centers of nCORE, a Semiconductor Research Corporation program, sponsored by National Institute of Standards and Technology (NIST), by the DARPA TEE program, and NSF Grant No. 1808190. This work used experimental facilities supported by NSF MRSEC Grant No. DMR1419807. We thank Professor Pietro Gambardella and Dr. Shulei Zhang for fruitful discussions.

*can.onur.avci@mat.ethz.ch

[1] K. Uchida, S. Takahashi, K. Harii, J. Ieda, W. Koshibae, K. Ando, S. Maekawa, and E. Saitoh, Nature (London) **455**, 778 (2008).
[2] K. Uchida, J. Xiao, H. Adachi, J. Ohe, S. Takahashi, J. Ieda, T. Ota, Y. Kajiwara, H. Umezawa, H. Kawai, G. E. W. Bauer, S. Maekawa, and E. Saitoh, Nat. Mater. **9**, 894 (2010).
[3] C. M. Jaworski, R. C. Myers, E. Johnston-Halperin, and J. P. Heremans, Nature (London) **487**, 210 (2012).
[4] T. Kikkawa, K. Uchida, Y. Shiomi, Z. Qiu, D. Hou, D. Tian, H. Nakayama, X.-F. Jin, and E. Saitoh, Phys. Rev. Lett. **110**, 067207 (2013).
[5] D. Qu, S. Y. Huang, J. Hu, R. Wu, and C. L. Chien, Phys. Rev. Lett. **110**, 067206 (2013).
[6] R. Ramos, T. Kikkawa, K. Uchida, H. Adachi, I. Lucas, M. H. Aguirre, P. Algarabel, L. Morellón, S. Maekawa, E. Saitoh, and M. R. Ibarra, Appl. Phys. Lett. **102**, 072413 (2013).

[7] S. M. Wu, J. E. Pearson, and A. Bhattacharya, Phys. Rev. Lett. **114**, 186602 (2015).
[8] S. M. Wu, W. Zhang, A. Kc, P. Borisov, J. E. Pearson, J. S. Jiang, D. Lederman, A. Hoffmann, and A. Bhattacharya, Phys. Rev. Lett. **116**, 097204 (2016).
[9] O. Mosendz, V. Vlaminck, J. E. Pearson, F. Y. Fradin, G. E. W. Bauer, S. D. Bader, and A. Hoffmann, Phys. Rev. B **82**, 214403 (2010).
[10] A. B. Cahaya, O. A. Tretiakov, and G. E. W. Bauer, IEEE Trans. Magn. **51**, 0800414 (2015).
[11] A. Kirihara, K. Kondo, M. Ishida, K. Ihara, Y. Iwasaki, H. Someya, A. Matsuba, K. I. Uchida, E. Saitoh, N. Yamamoto, S. Kohmoto, and T. Murakami, Sci. Rep. **6**, 23114 (2016).
[12] G. E. W. Bauer, E. Saitoh, and B. J. van Wees, Nat. Mater. **11**, 391 (2012).
[13] M. Schmid, S. Srichandan, D. Meier, T. Kuschel, J.-M. Schmalhorst, M. Vogel, G. Reiss, C. Strunk, and C. H. Back, Phys. Rev. Lett. **111**, 187201 (2013).
[14] M. Schreier, N. Roschewsky, E. Dobler, S. Meyer, H. Huebl, R. Gross, and S. T. B. Goennenwein, Appl. Phys. Lett. **103**, 242404 (2013).
[15] N. Vlietstra, J. Shan, B. J. van Wees, M. Isasa, F. Casanova, and J. Ben Youssef, Phys. Rev. B **90**, 174436 (2014).
[16] H. Nakayama, M. Althammer, Y. T. Chen, K. Uchida, Y. Kajiwara, D. Kikuchi, T. Ohtani, S. Geprägs, M. Opel, S. Takahashi, R. Gross, G. E. W. Bauer, S. T. B. Goennenwein, and E. Saitoh, Phys. Rev. Lett. **110**, 206601 (2013).
[17] C. Hahn, G. de Loubens, O. Klein, M. Viret, V. V. Naletov, and J. Ben Youssef, Phys. Rev. B **87**, 174417 (2013).
[18] N. Vlietstra, J. Shan, V. Castel, B. J. van Wees, and J. Ben Youssef, Phys. Rev. B **87**, 184421 (2013).
[19] C. O. Avci, A. Quindeau, M. Mann, C. F. Pai, C. A. Ross, and G. S. D. Beach, Phys. Rev. B **95**, 115428 (2017).
[20] D. J. Kim, C. Y. Jeon, J. G. Choi, J. W. Lee, S. Surabhi, J. R. Jeong, K. J. Lee, and B. G. Park, Nat. Commun. **8**, 1400 (2017).
[21] K. Tauber, M. Gradhand, D. V. Fedorov, and I. Mertig, Phys. Rev. Lett. **109**, 026601 (2012).
[22] S. Meyer, Y.-T. Chen, S. Wimmer, M. Althammer, T. Wimmer, R. Schlitz, S. Geprägs, H. Huebl, D. Ködderitzsch, H. Ebert, G. E. W. Bauer, R. Gross, and S. T. B. Goennenwein, Nat. Mater. **16**, 977 (2017).
[23] P. Sheng, Y. Sakuraba, S. Takahashi, and S. Mitani, Sci. Adv. **3**, e1701503 (2017).
[24] C. O. Avci, A. Quindeau, C.-F. Pai, M. Mann, L. Caretta, A. S. Tang, M. C. Onbasli, C. A. Ross, and G. S. D. Beach, Nat. Mater. **16**, 309 (2017).
[25] C. O. Avci, E. Rosenberg, M. Baumgartner, L. Beran, A. Quindeau, P. Gambardella, C. A. Ross, and G. S. D. Beach, Appl. Phys. Lett. **111**, 072406 (2017).
[26] J. Li, G. Yu, C. Tang, Y. Liu, Z. Shi, Y. Liu, A. Navabi, M. Aldosary, Q. Shao, K. L. Wang, R. Lake, and J. Shi, Phys. Rev. B **95**, 241305(R) (2017).
[27] Q. Shao *et al.*, Nat. Commun. **9**, 3612 (2018).
[28] C. O. Avci, E. Rosenberg, L. Caretta, F. Büttner, M. Mann, C. Marcus, D. Bono, C. A. Ross, and G. S. D. Beach, Nat. Nanotechnol. **14**, 561 (2019).
[29] A. Quindeau, C. O. Avci, W. Liu, C. Sun, M. Mann, A. S. Tang, M. C. Onbasli, D. Bono, P. M. Voyles, Y. Xu, J. Robinson, G. S. D. Beach, and C. A. Ross, Adv. Electron. Mater. **3**, 1600376 (2017).
[30] E. R. Rosenberg, L. Beran, C. O. Avci, C. Zeledon, B. Song, C. Gonzalez-Fuentes, J. Mendil, P. Gambardella, M. Veis, C. Garcia, G. S. D. Beach, and C. A. Ross, Phys. Rev. Mater. **2**, 094405 (2018).
[31] See Supplemental Material at http://link.aps.org/supplemental/10.1103/PhysRevLett.124.027701 for supporting control measurements, discussion, and the quantification of device temperature and in-plane temperature gradients.
[32] L. J. Cornelissen, J. Liu, R. A. Duine, J. Ben Youssef, and B. J. Van Wees, Nat. Phys. **11**, 1022 (2015).
[33] S. T. B. Goennenwein, R. Schlitz, M. Pernpeintner, K. Ganzhorn, M. Althammer, R. Gross, and H. Huebl, Appl. Phys. Lett. **107**, 172405 (2015).
[34] J. Shan, P. Bougiatioti, L. Liang, G. Reiss, T. Kuschel, and B. J. Van Wees, Appl. Phys. Lett. **110**, 132406 (2017).
[35] C. O. Avci, K. Garello, M. Gabureac, A. Ghosh, A. Fuhrer, S. F. Alvarado, and P. Gambardella, Phys. Rev. B **90**, 224427 (2014).
[36] Y. Pu, D. Chiba, F. Matsukura, H. Ohno, and J. Shi, Phys. Rev. Lett. **101**, 117208 (2008).
[37] S. Geprägs, S. Meyer, S. Altmannshofer, M. Opel, F. Wilhelm, A. Rogalev, R. Gross, and S. T. B. Goennenwein, Appl. Phys. Lett. **101**, 262407 (2012).
[38] M. Althammer *et al.*, Phys. Rev. B **87**, 224401 (2013).
[39] T. Kuschel, C. Klewe, J. M. Schmalhorst, F. Bertram, O. Kuschel, T. Schemme, J. Wollschläger, S. Francoual, J. Strempfer, A. Gupta, M. Meinert, G. Götz, D. Meier, and G. Reiss, Phys. Rev. Lett. **115**, 097401 (2015).